

## Strain-mediated phase coexistence in MnAs heteroepitaxial films on GaAs: An x-ray diffraction study

V. M. Kaganer, B. Jenichen, F. Schippan, W. Braun, L. Däweritz, and K. H. Ploog  
Paul-Drude-Institut für Festkörperelektronik, Hausvogteiplatz 5-7, D-10117 Berlin, Germany

(Received 6 September 2001; published 10 July 2002)

The temperature-dependent phase coexistence between crystalline phases in heteroepitaxial films of MnAs on GaAs is studied. The epitaxial constraints on the film expansion are analyzed. The x-ray-diffraction data are fitted to a model of periodic elastic domains. The temperature dependencies of phase fractions, the domain sizes, and the misfits are simultaneously obtained. The domain sizes correspond to the minimum of elastic energy, which proves the equilibrium state of the heteroepitaxial system at each temperature.

DOI: 10.1103/PhysRevB.66.045305

PACS number(s): 68.35.Rh, 64.70.Kb, 61.50.Ks, 05.70.Np

### I. INTRODUCTION

Recently we found<sup>1</sup> that a first-order structural phase transition in MnAs heteroepitaxial films on GaAs proceeds in a way qualitatively different from the same transition in bulk MnAs crystals. Instead of an abrupt transition with a temperature hysteresis inherent to the first-order transition in bulk crystals, we have observed a phase coexistence in a temperature interval of more than 20 °C, with the fraction of the low-temperature phase linearly increasing on cooling and linearly decreasing on heating. We explained this phase coexistence by the restriction on lateral expansion of the film imposed by the substrate. The coexistence is a result of the balance between the free energy released at the phase transformation and the emerging elastic energy. In the present work, we perform a detailed x-ray-diffraction study of the temperature-dependent phase coexistence. We develop a model of periodic elastic domains in the layer, and find temperature dependencies of the phase fraction, misfit, and domain size by fitting the x-ray data to the model. We demonstrate, by comparing the observed domain structure with the energy-minimizing one, that the film is close to the equilibrium.

The formation of equilibrium polydomain structures as a way to reduce elastic energy at structural phase transformations in epitaxial films was first proposed theoretically by Roytburd.<sup>2</sup> The energetics of polydomain phases and equilibrium structures were considered further by Bruinsma and Zangwill,<sup>3</sup> Kwak and co-workers,<sup>4,5</sup> Speck and co-workers,<sup>6-9</sup> Sridhar and co-workers,<sup>10,11</sup> Roytburd and co-workers,<sup>12-15</sup> and Bratkovsky and Levanyuk.<sup>16,17</sup> Most of the cited papers concentrate on the phase transformation consisting in a tetragonal distortion of a cubic crystal (interchangeably referred to as martensitic, ferroelectric, or ferroelastic phase transformation). At this transition, the elastic energy is minimized by a coexistence of domains (twins) with three orthogonal directions of the tetragonal distortion. The orientations of domain boundaries are determined by crystallographic orientations of neutral planes which allow one to fit phases without strain at the boundary.<sup>2</sup> A possible coexistence between the parent and a derivative phase was considered theoretically by Roytburd and co-workers<sup>12-15</sup> assuming that the period of the domain structure is smaller

than the thickness of the film. This assumption is not applicable for the experimental system studied in the present work. We therefore develop a theory which is not limited in the domain widths.

MnAs on GaAs is a promising heteroepitaxial system which integrates magnetic and semiconductor properties. One of the aims in combining such materials is to inject spin-polarized electrons into a semiconductor.<sup>18</sup> The structure of bulk MnAs crystals,<sup>19-22</sup> the epitaxial relationships of MnAs on GaAs,<sup>23-27</sup> and the structure of the interface<sup>28,29</sup> are known. Figure 1 sketches the epitaxy of MnAs on a GaAs(001) surface. The hexagonal prism of the MnAs unit cell is attached to the GaAs(001) surface by a side facet. Epitaxial growth proceeds despite a large mismatch along the *c* axis of the prism which amounts to 33%. Transmission electron microscopy studies<sup>28,29</sup> showed that every sixth GaAs{220} plane fits into every fourth MnAs{0002} plane, which reduces the actual mismatch to 5%. This mismatch, as well as the mismatch along the perpendicular direction (7.7%), are released by regular arrays of misfit dislocations. The MnAs films are grown<sup>28,29</sup> with a unique epitaxial orientation with respect to the polar GaAs(001) surface, namely,  $(\bar{1}100)$  MnAs  $\parallel$  (001) GaAs and  $[0001]$  MnAs  $\parallel$   $[[1\bar{1}0]$  GaAs, which was checked in the present study by *in situ* reflection high-energy electron diffraction. It is essential for the considerations below that the orientation of the film with respect to the substrate is unique. There are no rotationally equivalent domains (twins), albeit translational domains can be present.

The crystal structure of the bulk MnAs phases and the phase diagram of MnAs were reviewed in Refs. 30-32. Below 40 °C, the bulk MnAs crystal is ferromagnetic and forms

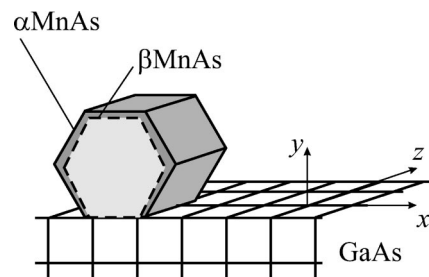


FIG. 1. Scheme of the epitaxy of MnAs on GaAs(001).

the hexagonal  $\alpha$ MnAs phase. At approximately 40 °C, the bulk  $\alpha$ MnAs undergoes a first-order phase transition to the paramagnetic orthorhombic phase  $\beta$ MnAs. Its unit cell is shown in Fig. 1 by the dashed line: the hexagon anisotropically shrinks in both directions, while the height of the prism does not change. The orthorhombic distortion of the  $\beta$ MnAs unit cell is small<sup>20</sup> ( $<0.2\%$ ). The transition is accompanied by a large ( $\approx 1.2\%$ ) lattice parameter discontinuity in the hexagonal plane and a large ( $\approx 15^\circ\text{C}$ ) temperature hysteresis. The discontinuous ferromagnetic transition (while magnetic phase transitions are commonly continuous at Curie temperature) is explained by strong magnetostriction effects.<sup>33</sup> A further phase transition in bulk MnAs takes place at 125 °C. This transition is continuous and results in a paramagnetic  $\gamma$ MnAs phase, which is again hexagonal. The successive phase transformations in MnAs can be explained with the Landau theory involving two coupled order parameters responsible for the orthorhombic distortion and magnetization.<sup>34</sup> The magnetostriction suppresses distortion at the ferromagnetic transition.

## II. THEORY

### A. Phase transition under mean-strain constraint

An epitaxial film experiencing a structural phase transformation cannot freely change its size and shape, as is possible for a bulk single crystal, but is the subject of several constraints. One of them is an integral constraint imposed on the whole film: the film cannot change its lateral size and hence the mean lateral lattice spacing in the film is constant. This requirement gives rise to elastic strain in the film and results in the phase coexistence at the first-order phase transformation,<sup>1</sup> but does not restrict the domain sizes of the coexisting phases. This is considered in the present subsection.

Further constraints are local and follow from the lattice continuity at the interfaces between the film and the substrate and between the domains. The latter requirement determines the orientation of the boundaries between domains of tetragonal phase at the martensitic (ferroelectric) transition as planes of zero misfit.<sup>2</sup> The present paper deals with the uniform dilatation in the hexagonal plane of the film, and strain at the domain boundaries is unavoidable. The calculation of the displacement field, the minimization of the elastic energy, and the calculation of the x-ray-diffraction pattern are presented in the subsequent subsections.

We adopt the notation to the  $\alpha$ MnAs- $\beta$ MnAs transition, which is studied experimentally in the present paper, and refer to the high-temperature phase as the  $\beta$  phase and the low-temperature phase as  $\alpha$  phase. We take the substrate unit cell as a reference. First consider the film in a single-phase state (either the  $\alpha$  or  $\beta$  phase) detached from the substrate, so that the film is free to expand. Then the relative differences between lattice spacings of the substrate and those of the corresponding phase in a *free* MnAs single crystal can be described by the tensors  $\hat{\eta}_\alpha$  and  $\hat{\eta}_\beta$ , commonly called internal strain tensors. The difference  $\hat{\eta} = \hat{\eta}_\alpha - \hat{\eta}_\beta$  consists of the

phase transformation strain and the difference between thermal expansions of the two phases.

The latter contribution cannot be neglected for the  $\alpha$ MnAs- $\beta$ MnAs transition, since the  $\alpha$ MnAs phase experiences thermal contraction, while  $\beta$ MnAs thermally expands. The values of the corresponding thermal coefficients<sup>19-22</sup> are of the order of  $10^{-4}\text{K}^{-1}$ , i.e., very large compared to the thermal expansion coefficient of the GaAs substrate which is<sup>35</sup>  $6 \times 10^{-6}\text{K}^{-1}$ . The shear components of the misfit are absent in the problem under consideration, and hence all off-diagonal components of  $\hat{\eta}_\alpha$  and  $\hat{\eta}_\beta$  are zero. We take into account that the lattice parameters at the  $\alpha$ MnAs- $\beta$ MnAs transition are discontinuous only in the hexagonal plane, so that  $\eta_{zz} = 0$ . Orientation of the axes is shown in Fig. 1: the  $y$  axis is normal to the film, and  $x$  and  $z$  axes are in the film plane. We neglect the small orthorhombic distortion of the  $\beta$ MnAs phase compared to the change of the lattice parameter at the transition and take  $\eta_{\alpha xx} - \eta_{\beta xx} = \eta_{\alpha yy} - \eta_{\beta yy} \equiv \eta$ . These simplifications allow us to present the results in a compact form.

The free film can be coherently attached to the substrate if an external stress is applied to the film, to make the film and substrate lattices match along the interface. After the film is attached and the external stress is removed, the film becomes elastically strained. The coexistence of the  $\alpha$  and  $\beta$  phases is a way to minimize the elastic energy under the constraint of the constant lateral size of the film imposed by epitaxy. Let  $\hat{e}_\alpha$  and  $\hat{e}_\beta$  be the elastic strain tensors in the corresponding phases. Then the relative change of the lattice spacing of the film in the corresponding phase with respect to the substrate is given by the sum of the internal and the elastic strain  $\hat{e}_a = \hat{\eta}_a + \hat{e}_a$  ( $a = \alpha$  or  $\beta$ ), which is called the total strain.

Let  $\xi$  be the fraction of the  $\alpha$  phase in the film. The lateral size of the epitaxial film is restricted by the substrate, and hence the lateral components of the mean total strain in the film are equal to zero:

$$\begin{aligned}\xi \varepsilon_{\alpha xx} + (1 - \xi) \varepsilon_{\beta xx} &= 0, \\ \xi \varepsilon_{\alpha zz} + (1 - \xi) \varepsilon_{\beta zz} &= 0.\end{aligned}\tag{1}$$

In this subsection, we do not take into consideration the interfaces between the substrate and the film and between the domains of the film. Then the free-energy density of the film consists of the free-energy densities of the phases in the unstrained state,  $f_\alpha$  and  $f_\beta$ , and the elastic energy densities  $E_\alpha$  and  $E_\beta$ :

$$f = \xi(f_\alpha + E_\alpha) + (1 - \xi)(f_\beta + E_\beta).\tag{2}$$

The elastic energy densities of the phases can be expressed through the elastic strains  $\hat{e}_\alpha$  and  $\hat{e}_\beta$ . The absence of the stress normal to the film  $\sigma_{yy} = 0$  relates the strain components:  $e_{\alpha yy} = -[\nu/(1 - \nu)](e_{\alpha xx} + e_{\alpha zz})$ , where  $a = \alpha$  or  $\beta$  and  $\nu$  is the Poisson ratio. The film is assumed to be elastically isotropic. Then the elastic energy density of each phase is

$$E_a = Y(e_{\alpha xx}^2 + 2\nu e_{\alpha xx} e_{\alpha zz} + e_{\alpha zz}^2),\tag{3}$$

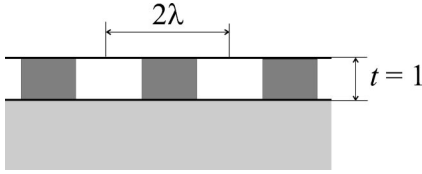


FIG. 2. Scheme of a periodic domain structure with alternating domains of two phases. The period of the domain structure is  $2\lambda$ .

where  $Y = Y_0/2(1 - \nu^2)$ , and  $Y_0$  is the Young modulus.

We substitute the elastic strains  $\hat{e}_a = \hat{\epsilon}_a - \hat{\eta}_a$  ( $a = \alpha, \beta$ ) into Eqs. (3) and, using Eqs. (1), find the minimum of the free energy density [Eq. (2)] with respect to the total strains at a given fraction  $\xi$  of the  $\alpha$  phase. The result is

$$f = f_\beta + \xi \Delta f + Y \xi^2 \eta^2, \quad (4)$$

where

$$\Delta f = f_\alpha - f_\beta + 2Y \eta (\eta_{\beta xx} + \nu \eta_{\beta zz}). \quad (5)$$

The bulk phase transition temperature  $T_c$  is determined by the condition  $f_\alpha = f_\beta$ . The difference between the free-energy densities in the two phases  $f_\alpha - f_\beta$  is a linear function of the temperature close to the transition,  $f_\alpha - f_\beta = Q(T - T_c)/T_c$ , where  $Q$  is the latent heat. The last term of Eq. (5) shifts the transition temperature in the film with respect to the bulk transition temperature. We denote the transition temperature in the film by  $T_c^*$ .

The minimum of the free energy density [Eq. (4)] is achieved by the phase coexistence with a fraction of the  $\alpha$  phase:

$$\xi = -\frac{\Delta f}{2Y\eta^2} = \frac{Q}{2Y\eta^2} \frac{T_c^* - T}{T_c^*}. \quad (6)$$

The temperature range of the phase coexistence is limited by the condition  $0 < \xi < 1$ . Therefore, the low-temperature  $\alpha$  phase appears at the temperature  $T_c^*$  and its fraction almost linearly increases when the temperature is decreased below  $T_c^*$ . Some nonlinearity is introduced by the temperature dependence of  $\eta$  which arises from the thermal expansion of the phases.<sup>1</sup> We can estimate the temperature interval of the phase coexistence  $\Delta T = 2Y\eta^2 T_c^*/Q$  using the values of latent heat<sup>36</sup>  $Q = 1.8$  cal/g, Young modulus<sup>37</sup>  $Y_0 = 3.2 \times 10^{11}$  dyn/cm<sup>2</sup>, the internal strain  $\eta = 0.01$ , and the transition temperature  $T_c^* = 320$  K as  $\Delta T \approx 20$  K, which is in a good agreement with the experimental results presented below.

The mean-strain constraint [Eq. (1)] gives rise to the finite temperature interval of the phase coexistence, but does not restrict the domain sizes of the coexisting phases. We now turn to this more elaborate problem, which requires a complete treatment of the compatibility between the domains and between the film and the substrate.

### B. Elastic domains

We consider an epitaxial film with a periodic array of elastic domains of two alternating phases, Fig. 2. The thick-

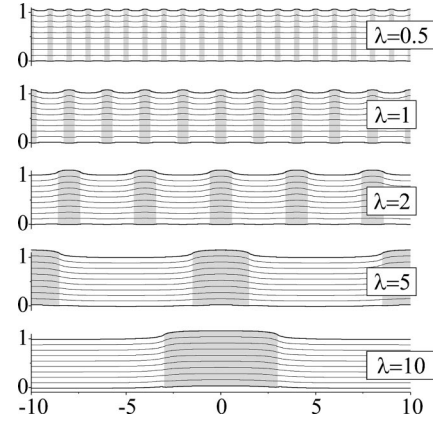


FIG. 3. The normal displacements in the film calculated by Eqs. (7) and (8) for different periods of domain structure  $2\lambda$ . The phase fraction is  $\xi = 0.3$  for all plots. The misfit between phases  $\eta = 0.01$ , the displacement  $u_y$  is magnified by a factor of 10.

ness  $t$  of the film is taken as the length unit. The period of the domain structure is  $2\lambda$  (in units of  $t$ ) and the domain boundaries are normal to the film. The elastic problem for this domain geometry with arbitrary internal strain tensors was solved by Sridhar, Rickman, and Srolovitz.<sup>10,11</sup> In brief, the solution consists of a Fourier expansion of the periodic internal strain and solution of the elastic equilibrium problem for each Fourier component. The elastic equilibrium equation  $\partial \sigma_{ij} / \partial x_j = 0$  is solved in the film where the stress  $\hat{\sigma}$  is caused by the elastic strain  $\hat{\epsilon} - \hat{\eta}$  and in the substrate where the internal strain  $\hat{\eta}$  is zero. The boundary conditions are given at the free surface (tractions are absent), at the film-substrate interface (displacements and tractions are continuous), and in the substrate far away from the interface (stress vanishes). We repeat the calculations since we need the displacement field in the film  $u_y(x, y)$  while only the elastic energy is given in the cited papers. We calculate the elastic energy for the diagonal components of the internal strain tensors and found only one minor error in the final formulas of Ref. 10: in the coefficient  $\alpha_7$  in Eq. (B1) of Ref. 10 read  $2\nu\delta_{11}\delta_{22}$  instead of  $2\nu\delta_{11}\delta_{22}$ . The final expression for the normal displacement  $u_y$  reads

$$u_y = \frac{\eta}{1-\nu} \left[ (1-\xi)y + \sum_{n=1}^{\infty} c_n \frac{(-1)^n}{\pi n} \sin(\pi n \xi) \cos \frac{\pi n x}{\lambda} \right], \quad (7)$$

where

$$c_n = a_n \exp \left[ - (1-y) \frac{\pi n}{\lambda} \right] - \frac{\lambda}{\pi n} \exp \left( -y \frac{\pi n}{\lambda} \right),$$

$$a_n = 2 + 4(1-\nu) \frac{\lambda}{\pi n} - \left( (3-4\nu) \frac{\lambda}{\pi n} + 2 \right) e^{-\pi n/\lambda} + 2y(e^{-\pi n/\lambda} - 1). \quad (8)$$

Figure 3 shows the normal displacements  $u_y(x, y)$  which are calculated by Eqs. (7) and (8) for different periods of the domain structure  $2\lambda$ . When the domains are narrow ( $\lambda$

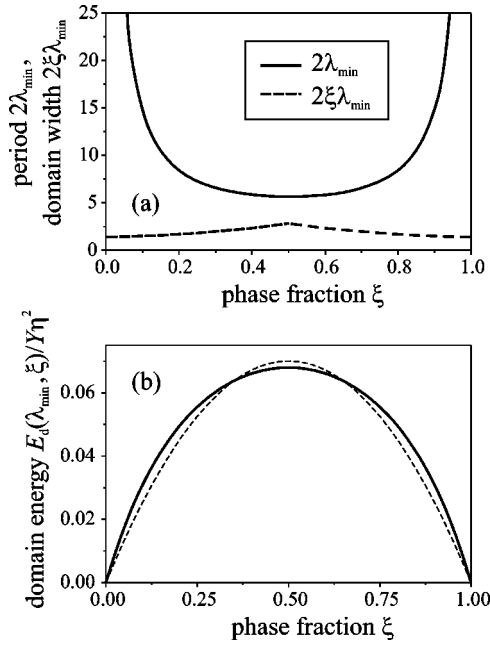


FIG. 4. (a) Period of the domain structure minimizing the elastic energy  $2\lambda_{\min}$  (full line) and the width of a smaller domain [equal to  $2\xi\lambda_{\min}$  for  $\xi < 1/2$  and  $2(1-\xi)\lambda_{\min}$  for  $\xi > 1/2$ , broken lines]. (b) Elastic energy for the energy-minimizing period,  $E_d(\lambda_{\min}, \xi)$  (full line) and its approximation by a parabola (broken line).

$< 1$ ), the coherence at the interfaces between the domains results in a common lattice spacing for the two phases in the film's interior. In contrast, when the domains are wide ( $\lambda \gg 1$ ), the spacings differ from each other and are close to the free spacings in the corresponding phases. We show in Sec. II C that this dependence of the spacing on the domain period makes the x-ray-diffraction pattern sensitive to the domain widths.

The expression for the elastic energy<sup>10,11</sup> is significantly simplified for the case under consideration ( $\eta_{xx} = \eta_{yy} \equiv \eta$ ,  $\eta_{zz} = 0$ ). We find that the free energy density [Eq. (4)] is supplemented with an additional term which depends on the period of the domain structure:

$$E_d = 2Y\eta^2 \sum_{n=1}^{\infty} \left[ 1 - \frac{2\lambda}{\pi n} (1 - e^{-\pi n/\lambda})^2 \right] \frac{\sin^2(\pi n \xi)}{(\pi n)^2}. \quad (9)$$

The energy  $E_d(\lambda, \xi)$  for a fixed phase fraction  $\xi$  has a minimum at some finite value of the period  $2\lambda_{\min}(\xi)$ . This period is shown in Fig. 4(a) as function of the phase fraction. It diverges at  $\xi = 0$  and 1 and reaches the minimum of 5.65 at  $\xi = 1/2$ . The width of the smaller domain, equal to  $2\xi\lambda_{\min}$  for  $\xi < 1/2$  and  $2(1-\xi)\lambda_{\min}$  for  $\xi > 1/2$ , remains finite and varies from 1.4 at  $\xi = 0$  and 1 to 2.8 for  $\xi = 1/2$ .

The energy-minimizing domain period  $2\lambda_{\min}$  is a result of a competition between the coherence requirements at the film—substrate interface and at the interfaces between the domains in the film. The coherence at the film-substrate interface favors narrow domains, since they localize strains near the interface in a layer with a thickness comparable to the domain width.<sup>12–15</sup> On the other hand, for narrow do-

main the coherence at the interfaces between domains requires equal spacings in the direction normal to the film, while for wide domains the elastic strains in that direction (i.e.,  $e_{yy}$ ) relax independently in the two phases. The optimum is realized with domain widths comparable with the film thickness.

Figure 4(b) shows the elastic energy density for the energy-minimizing period,  $E_d(\lambda_{\min}, \xi)$ . The broken line is an approximation of this energy by a parabola

$$E_d(\lambda_{\min}, \xi) \approx 0.28Y\eta^2\xi(1-\xi). \quad (10)$$

Adding this energy to Eq. (4), we find that the domain energy increases the temperature range of phase coexistence by a factor  $(1-0.28)^{-1} \approx 1.4$  and also causes an additional shift of the transition temperature with respect to the bulk transition.

### C. X-ray scattering from elastic domains

The x-ray diffraction from the film can be calculated by using the kinematic scattering formula

$$\mathcal{I}(q_x, q_y) = \left| \int \exp[i\mathbf{Q} \cdot \mathbf{u}(x, y) + i(q_x x + q_y y)] dx dy \right|^2, \quad (11)$$

where  $q_x$  and  $q_y$  are the deviations of the scattering vector from the reciprocal-lattice vector  $\mathbf{Q}$  and the integration is performed over the film thickness and one period of its lateral structure. We consider only the symmetric Bragg reflections (vector  $\mathbf{Q}$  is parallel to the  $y$  axis), and the vertical displacement  $u_y(x, y)$  given by Eqs. (7) and (8) is sufficient for the calculations. The sharp surfaces of the film give rise to thickness intensity oscillations while the domain periodicity leads to satellite peaks. These features are not seen in the experiments presented below because of film thickness variations, misorientation of different parts of the film (mosaicity), nonideal periodicity of the domains, and the finite angular resolution of the experiment. Therefore, we do not attempt to calculate the satellite peaks and average the thickness intensity oscillations by taking into account the film mosaicity and the angular resolution of the detector.

Let  $\phi$  be the angular deviation of the diffracted beam from the reference geometry and  $\psi$  the deviation of the film normal from the reference orientation. The corresponding deviation of the wave vectors are  $\delta q_x = k(\psi + \phi \sin \theta)$  and  $\delta q_y = k\phi \cos \theta$ , where  $k$  is the wave vector and  $\theta$  is the Bragg angle. We consider the  $\omega - 2\theta$  scan in the experiment and take  $q_x = 0$  in the reference geometry. Then the average of the intensity (11) with the detector resolution function  $R_d(\phi)$  and the film mosaicity distribution  $R_m(\psi)$  is

$$I(q_y) = \int \mathcal{I}(q'_x, q'_y) R_d \left( \frac{q'_y - q_y}{k \cos \theta} \right) \times R_m \left( \frac{q'_x - (q'_y - q_y) \tan \theta}{k} \right) dq'_x dq'_y. \quad (12)$$

Figure 5 presents the x-ray-diffraction peaks calculated by using Eqs. (7), (8), (11), and (12) for the same domains as

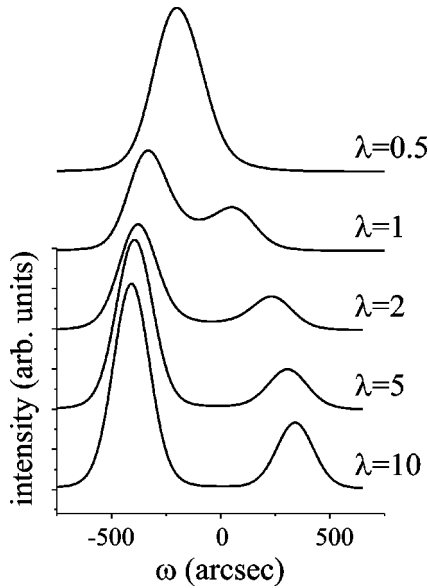


FIG. 5. Calculated x-ray-diffraction peaks for different periods of the domain structure. ( $\bar{1}100$ ) reflection from MnAs, the phase fraction  $\xi=0.3$ , film thickness  $t=180$  nm, phase transformation strain  $\eta=0.01$ , angular resolution of detector  $\Delta\phi=0.1^\circ$  and film misorientation  $\Delta\psi=0.1^\circ$ .

shown in Fig. 3. The diffraction pattern qualitatively changes as  $\lambda$  is changed. Only one diffraction peak is seen for  $\lambda < 1$ , since the coherence between the domains whose width is essentially smaller than the film thickness results in a common lattice spacing for both phases. The separation between the peaks gradually increases for  $\lambda \geq 1$  and reaches (for  $\lambda \geq 1$ ) a limiting value given by the mean-strain constraint. We conclude that the diffraction pattern is sensitive to the domain period.

### III. EXPERIMENT

The MnAs layers were grown<sup>28</sup> by solid source molecular-beam epitaxy on 100-nm-thick GaAs buffer layers at  $250^\circ\text{C}$  with a growth rate of  $19 \text{ nm h}^{-1}$ . The GaAs substrate wafers were soldered with indium onto the Mo substrate holder. The x-ray measurements on samples 1, 2, and 3 (the thicknesses of the MnAs film were 60, 120, and 180 nm, respectively) were performed on the as-grown samples. For samples 4 and 5 (the thicknesses of the MnAs films were 100 and 180 nm), the soldering In layer was removed by thinning the sample from the back side to thicknesses of 330 and  $267 \mu\text{m}$ , respectively.

The x-ray-diffractometric measurements were performed in a high-resolution x-ray diffractometer with temperature controlled sample stages described below using a symmetrically cut four-reflection Du Mond–Bartels type Ge 220 monochromator placed at a distance of 30 cm from the sample and  $\text{CuK}\alpha_1$  radiation. The angular acceptance of the detector was  $0.1^\circ$ .

The working temperature at the diffractometer was  $30^\circ\text{C}$ . The measurements above that temperature were performed by using a resistive heating. It was sufficient for the whole

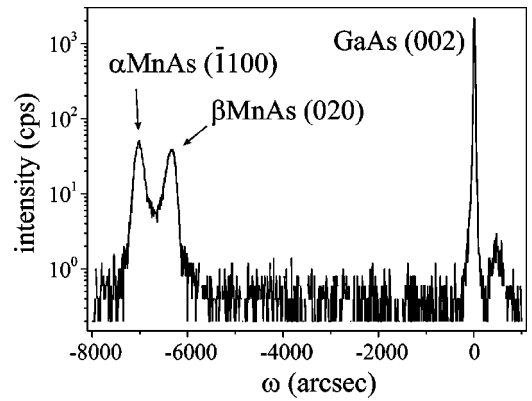


FIG. 6. Diffraction curve ( $\omega-2\theta$  scan) near the GaAs (002) reflection measured at a temperature of  $30^\circ\text{C}$  on sample 5 (Cu  $K\alpha_1$  radiation). The  $\alpha\text{MnAs}(\bar{1}100)$  and the  $\beta\text{MnAs}(020)$  reflections are clearly distinguished.

set of measurements on samples 1 and 2. Sample 3 was also studied under cooling with a separate circulating-fluid device. Samples 4 and 5 were studied with the aid of a combined device with resistive heating and cooling by liquid nitrogen. The estimated systematic uncertainty in temperature determination was at most  $2^\circ\text{C}$ . The curvatures of samples 4 and 5, caused by the misfit between the MnAs film and the GaAs substrate, were measured in a double crystal topographic camera equipped with a plane Si 440 collimator crystal<sup>38</sup> by observing the displacement of the diffraction spot (GaAs 135 or 115) over the sample surface with the change of the incidence angle.

### IV. RESULTS

Figure 6 presents the  $\omega-2\theta$  diffractometric curve recorded on sample 5 at  $30^\circ\text{C}$ . Besides the strong substrate peak (GaAs 002) two closely spaced peaks of the MnAs film are visible. These peaks are the  $\bar{1}100$  peak of  $\alpha\text{MnAs}$  and 020 peak of  $\beta\text{MnAs}$ . We use the hexagonal notation of the reflections for  $\alpha\text{MnAs}$  and the orthorhombic notation for  $\beta\text{MnAs}$ . If the small orthorhombic distortion is neglected, the 020 peak of  $\beta\text{MnAs}$  can also be referred to as the  $\bar{1}100$  peak. The latter notation is used in Fig. 5, where the peaks of two phases are calculated.

A weak peak on the right from the substrate peak is the MnAs  $\bar{1}101$  peak originating from a small fraction of the film grown in  $\bar{1}101$  direction.<sup>25,27</sup> From the relative intensities of the peaks and the ratio of their structure factors ( $|f_{\bar{1}101}/f_{\bar{1}100}|^2 \approx 10.3$ ) we conclude that the fraction of the  $\bar{1}101$ -grown film is about 0.3% and can be ignored in the analysis below.

The MnAs peaks are shown in Fig. 7 in more detail and on a linear scale. A sequence of the  $\omega-2\theta$  diffractometric curves of sample 5 under stepwise cooling from  $55$  to  $7^\circ\text{C}$ , and subsequent heating is shown. The temperature was kept constant while recording each curve. The sample rotation angle  $\omega$  was measured with respect to the position of the GaAs 002 substrate peak; cf. Fig. 6. Only one peak of the

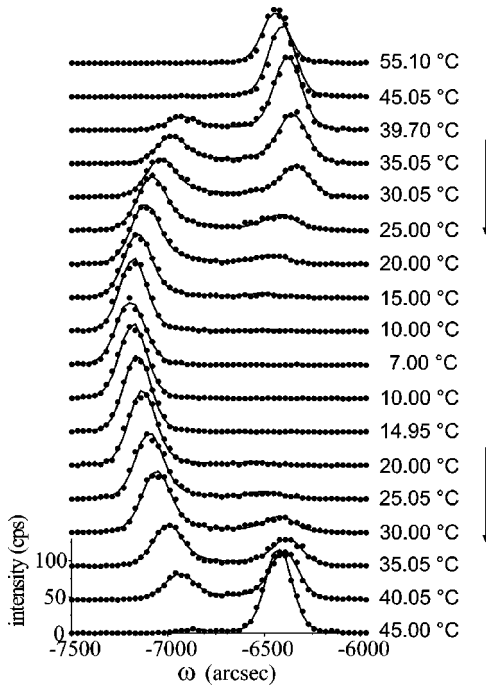


FIG. 7. Diffraction curves ( $\omega - 2\theta$  scans) of sample 5 obtained on cooling and heating the sample. The arrows in the right-hand part indicate the sequence of the measurements. The lines are the best fits to the model of periodic elastic domains.

$\beta$ MnAs phase is seen at high temperatures, and only the peak of the  $\alpha$ MnAs phase is present at low temperatures. At intermediate temperatures both peaks are observed, which points to a phase coexistence in a temperature range of more than 20 °C.<sup>1</sup> The fraction of the  $\alpha$ MnAs phase continuously decreases upon cooling and continuously increases upon heating. The diffractometric curves are reproduced on thermal cycling without any change, which points to the equilibrium nature of the observed phase coexistence.

The lines in Fig. 7 are the best fits of the curves to the intensity calculated by Eqs. (7), (8), (11), and (12). The parameters of fit are the phase fraction  $\xi$ , the domain period  $2\lambda$ , the misfit between the phases of the film  $\eta = \eta_{\alpha xx} - \eta_{\beta xx}$ , the difference of lattice spacings (normal to the film) between the  $\alpha$ MnAs phase of the film and the substrate

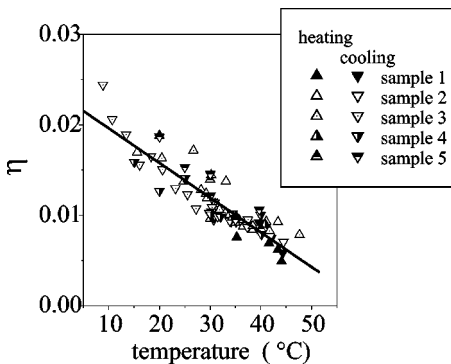


FIG. 8. The misfit between  $\alpha$ MnAs and  $\beta$ MnAs phases as a function of temperature.

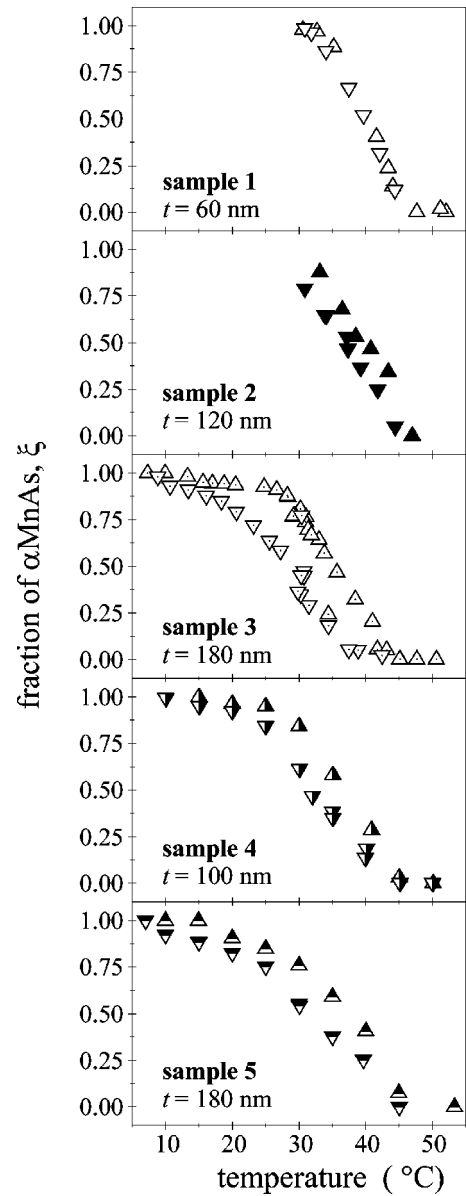


FIG. 9. Fractions of  $\alpha$ MnAs phase obtained on heating (up triangles) and cooling (down triangles) of the samples. The thickness  $t$  of the MnAs films is indicated.

$\epsilon_y = (\eta_{\alpha xx} + \nu \eta_{\alpha zz}) / (1 - \nu)$ , the peak intensity which is a scaling factor, and the intensity background. All these parameters depend on the temperature. Fortunately, different fit parameters are sensitive to different features of the diffraction curve, which allows one to obtain them from one fit. The relative integral intensities of the two peaks are given by the phase fraction  $\xi$ . The distance between the peaks depends on the misfit between phases of the film  $\eta$  and the domain period  $2\lambda$ . The depth of the minimum between the peaks is sensitive to  $\lambda$ . The misfit to the substrate  $\epsilon_y$  is given by the peak positions with respect to the substrate peak.

Figure 8 shows the temperature dependence of the misfit between the MnAs phases  $\eta$  obtained from the fits of the diffraction curves of all five samples on cooling and heating. The experimental points follow a linear temperature dependence  $\eta = 0.023 - 3.84 \times 10^{-4} T [^\circ\text{C}]$ . The temperature gra-

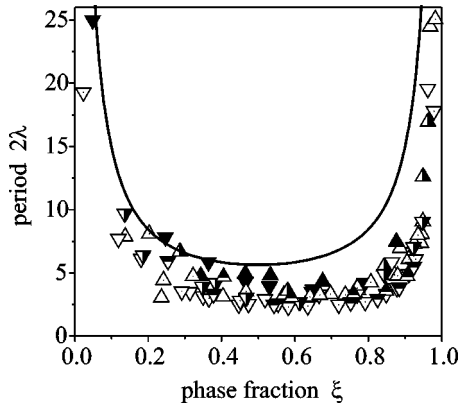


FIG. 10. Period of the domain structure  $2\lambda$  obtained by the fit of the x-ray data to the model of periodic domains. Up and down triangles denote the measurements on heating and cooling the samples, respectively. Samples 1–5 are denoted by the same symbols as in Figs. 8 and 9. The solid line is the result of energy minimization presented in Fig. 4(a).

gradient of  $\eta$  is in a good agreement with the difference between thermal contraction of the  $\alpha$ MnAs phase and thermal expansion of the  $\beta$ MnAs phase.<sup>19,21,22</sup> Further fits were performed taking this linear dependence of  $\eta$  and excluding  $\eta$  from the list of fit parameters. These did not change the results essentially but somewhat reduced scattering of the points.

Figure 9 presents the temperature dependencies of the fraction  $\xi$  of the  $\alpha$ MnAs phase. This parameter is rather insensitive to the fit model. It can be found simply from the ratio of the integrated intensities of the peaks.<sup>1</sup> The fraction of the  $\alpha$ MnAs phase increases on cooling almost linearly in all samples in the temperature intervals of 15 to 25 °C. The phase coexistence is explained by the theory presented above. The phase coexistence is accompanied by a temperature hysteresis in all samples with the exception of sample 1. The maximum hysteresis of 7 °C is found in sample 3. It is worth to note that the hysteresis in Fig. 9 cannot be explained in the same way as usual temperature hysteresis at a first order phase transition caused by the absence of nucleation sites of the new phase.<sup>33</sup> In the system under consideration, both phases are present at any temperature in the phase coexistence range in comparable, albeit different, amounts. The change of the phase fraction proceeds without nucleation by a barrierless motion of the domain walls.

Figure 10 presents the domain period  $2\lambda$  obtained from the fit of the diffraction peaks. The period plotted versus the phase fraction  $\xi$  does not show a hysteresis which would be present on a  $\lambda(T)$  plot. The data from all samples fall on a common curve and well agree with the domain period found from the elastic energy minimum in Sec. II B. The agreement between the domain periods found from the x-ray-diffraction data and by elastic energy minimization proves the equilibrium nature of the phase coexistence.

Figure 11 shows the temperature dependence of the difference of lattice spacings between the  $\alpha$ MnAs phase of the film and the substrate in the direction of the normal to the film,  $\epsilon_y = (\eta_{\alpha xx} + \nu \eta_{\alpha zz}) / (1 - \nu)$ . The data from all five

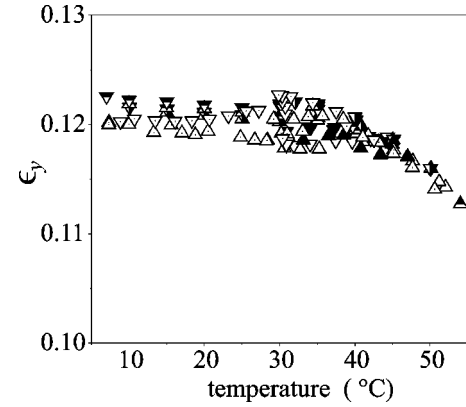


FIG. 11. Relative difference  $\epsilon_y$  between the  $(1\bar{1}00)$   $\alpha$ MnAs and  $(002)$  GaAs lattice spacings perpendicular to the surface in samples 1–5. Note that the scale is chosen the same as in Fig. 8.

samples fall on a common curve. The temperature gradient of  $\epsilon_y$  is much smaller than that of the misfit between the phases  $\eta$  shown in Fig. 8 (note that the abscissas in Figs. 8 and 11 give the same intervals of values). Such a temperature dependence results from the compensation of the thermal expansion along the  $c$  axis ( $\eta'_{\alpha zz} > 0$ , where the prime denotes the temperature derivative) by the thermal contraction in the hexagonal plane ( $\eta'_{\alpha xx} < 0$ ) and indicates that  $\eta'_{\alpha xx} \approx -\nu \eta'_{\alpha zz}$ . This conclusion is in an agreement with measurements of the temperature dependencies of the MnAs lattice parameters in bulk crystals,<sup>21,22</sup> which give the ratio  $\eta'_{\alpha xx} / \eta'_{\alpha zz}$  in the range  $-1/3$  to  $-1/2$ .

The lateral misfit between the film and the substrate can be calculated from the sample curvature measurements. Table I presents the results of the curvature measurements of samples 4 and 5 at 30 °C. The curvature radii are maximum along the direction GaAs $[1\bar{1}0]$  (the  $c$  axis of the MnAs film) and minimum in the perpendicular direction (the hexagonal plane of the film). The curvature radii for intermediate directions follow the Euler theorem,  $1/R = \sin^2\gamma/R_a + \cos^2\gamma/R_c$ , where  $R_a$  and  $R_c$  are the curvature radii in the hexagonal plane and in the  $c$  direction of MnAs, respectively, and  $\gamma$  is

TABLE I. Radius of curvature  $R$  and lateral misfit  $\epsilon$  of the MnAs films at 30 °C in different directions.

| Sample | Reflection  | Angle to $c$ axis (degrees) | Curvature radius $R$ (m) | Misfit $\epsilon$ (%) |
|--------|-------------|-----------------------------|--------------------------|-----------------------|
| 4      | $1\bar{1}5$ | 0                           | 6.78                     | 2.7                   |
|        | 315         | 26                          | 7.77                     | 2.3                   |
|        | $3\bar{1}5$ | 74                          | 19.4                     | 0.94                  |
|        | 115         | 90                          | 32.82                    | 0.55                  |
| 5      | $1\bar{1}5$ | 0                           | 3.88                     | 1.7                   |
|        | 315         | 26                          | 2.9                      | 2.3                   |
|        | $3\bar{1}5$ | 74                          | 3.62                     | 1.8                   |
|        | 115         | 90                          | 38.8                     | 0.17                  |

the angle between the given direction in the surface plane and the  $c$  axis. The measured curvature radii allow one to calculate the lateral misfit  $\epsilon$  of the film with respect to the substrate in the corresponding directions by using Stoney's equation<sup>39,40</sup>

$$\frac{1}{R} = \frac{6t_f}{t_s^2} \epsilon, \quad (13)$$

where  $t_f$  and  $t_s$  are the film and substrate thicknesses ( $t_f \ll t_s$ ). We have  $t_f = 100$  nm and  $t_s = 330$   $\mu\text{m}$  for sample 4, and  $t_f = 180$  nm and  $t_s = 267$   $\mu\text{m}$  for sample 5. The values of the misfit in the hexagonal plane and in the  $c$  direction (i.e., in the two perpendicular directions parallel to the surface) are to be compared with the variations of the corresponding lattice parameters of MnAs in the temperature interval from 250 °C (the growth temperature) to room temperature, which are 0.6% and 1.5%, respectively.<sup>19</sup> We conclude that, at the growth temperature, the misfit is mostly relieved by networks of misfit dislocations. The thermal contraction of the GaAs substrate can be neglected, and the change of the lattice parameters of the MnAs film on cooling from the growth temperature is the dominant source of strain and sample bending at room temperature.

## V. CONCLUSIONS

We studied the first-order structural phase transformation in heteroepitaxial films of MnAs on GaAs. The substrate

does not allow the lateral expansion of the film, which results in the phase coexistence governed by a balance between the free energy released at the phase transformation and the emerging elastic energy. The local constraints on the coherence between the film and the substrate and between the two phases of the film define the domain sizes of the coexisting phases. We fitted the x-ray-diffraction data to the model of periodic elastic domains and simultaneously obtained the phase fractions, the domain sizes, and the misfits. We found that the fraction of the low-temperature  $\alpha\text{MnAs}$  phase linearly increases on cooling and linearly decreases on heating. The phase coexistence occurs in a temperature interval of 15–25 °C and is accompanied by a temperature hysteresis of 0–7 °C which probably points to imperfections of the samples. We found that the domain sizes correspond to the minimum of elastic energy, which proves that the heteroepitaxial system is at equilibrium at each temperature.

*Note added in proof.* The results of the present paper have been confirmed recently by direct observation of temperature-dependent periodic surface corrugations due to elastic domains of coexisting phases: see T. Plake, M. Ramsteiner, V. M. Kaganer, B. Jenichen, M. Kästner, L. Däweritz, and K. H. Ploog, *Appl. Phys. Lett.* **80**, 2523 (2002).

## ACKNOWLEDGMENTS

V.M.K. thanks M. Fradkin and A. Roytburd for helpful discussions.

- 
- <sup>1</sup>V.M. Kaganer, B. Jenichen, F. Schippan, W. Braun, L. Däweritz, and K.H. Ploog, *Phys. Rev. Lett.* **85**, 341 (2000).  
<sup>2</sup>A.L. Roytburd, *Phys. Status Solidi A* **37**, 329 (1976).  
<sup>3</sup>R. Bruinsma and A. Zangwill, *J. Phys. (Paris)* **47**, 2055 (1986).  
<sup>4</sup>B.S. Kwak, A. Erbil, B.J. Wilkens, J.D. Budai, M.F. Chisholm, and L.A. Boatner, *Phys. Rev. Lett.* **68**, 3733 (1992).  
<sup>5</sup>B.S. Kwak, A. Erbil, J.D. Budai, M.F. Chisholm, L.A. Boatner, and B.J. Wilkens, *Phys. Rev. B* **49**, 14 865 (1994).  
<sup>6</sup>W. Pompe, X. Gong, Z. Suo, and J.S. Speck, *J. Appl. Phys.* **74**, 6012 (1993).  
<sup>7</sup>J.S. Speck and W. Pompe, *J. Appl. Phys.* **76**, 466 (1994).  
<sup>8</sup>J.S. Speck, A. Seifert, W. Pompe, and R. Ramesh, *J. Appl. Phys.* **76**, 477 (1994).  
<sup>9</sup>J.S. Speck, A.C. Daykin, A. Seifert, A.E. Romanov, and W. Pompe, *J. Appl. Phys.* **78**, 1696 (1995).  
<sup>10</sup>N. Sridhar, J.M. Rickman, and D.J. Srolovitz, *Acta Mater.* **44**, 4085 (1996).  
<sup>11</sup>N. Sridhar, J.M. Rickman, and D.J. Srolovitz, *Acta Mater.* **44**, 4097 (1996).  
<sup>12</sup>A.L. Roytburd, *J. Appl. Phys.* **83**, 228 (1998).  
<sup>13</sup>A.L. Roytburd, *J. Appl. Phys.* **83**, 239 (1998).  
<sup>14</sup>S.P. Alpay and A.L. Roytburd, *J. Appl. Phys.* **83**, 4714 (1998).  
<sup>15</sup>A.L. Roytburd, T.S. Kim, Q. Su, J. Slutsker, and M. Wuttig, *Acta Mater.* **46**, 5095 (1998).  
<sup>16</sup>A.M. Bratkovsky and A.P. Levanyuk, *Phys. Rev. Lett.* **86**, 3642 (2001).  
<sup>17</sup>A.M. Bratkovsky and A.P. Levanyuk, *Phys. Rev. B* **65**, 094102 (2002).  
<sup>18</sup>H.J. Zhu, M. Ramsteiner, H. Kostial, M. Wassermeier, H.-P. Schönherr, and K.H. Ploog, *Phys. Rev. Lett.* **87**, 016601 (2001).  
<sup>19</sup>B.T.M. Willis and H.P. Rooksby, *Proc. Phys. Soc. London, Sect. B* **67**, 290 (1954).  
<sup>20</sup>R.H. Wilson and J.S. Kasper, *Acta Crystallogr.* **17**, 95 (1964).  
<sup>21</sup>G.A. Govor, *Fiz. Tverd. Tela (Leningrad)* **23**, 1444 (1981) [*Sov. Phys. Solid State* **23**, 841 (1981)].  
<sup>22</sup>G.A. Govor, K. Bärner, and J.-W. Schünemann, *Phys. Status Solidi A* **113**, 403 (1989).  
<sup>23</sup>M. Tanaka, J.P. Harbison, T. Sands, T.L. Cheeks, V.G. Keramidias, and G.M. Rothberg, *J. Vac. Sci. Technol.* **12**, 1091 (1994).  
<sup>24</sup>M. Tanaka, J.P. Harbison, M.C. Park, Y.S. Park, T. Shin, and G.M. Rothberg, *J. Appl. Phys.* **76**, 6278 (1994).  
<sup>25</sup>M. Tanaka, J.P. Harbison, M.C. Park, Y.S. Park, T. Shin, and G.M. Rothberg, *Appl. Phys. Lett.* **65**, 1964 (1994).  
<sup>26</sup>M. Tanaka, *Physica E (Amsterdam)* **2**, 372 (1998).  
<sup>27</sup>L. Däweritz, F. Schippan, A. Trampert, M. Kästner, G. Behme, Z. Wang, M. Moreno, P. Schützendübe, and K.H. Ploog, *J. Cryst. Growth* **227-228**, 834 (2001).  
<sup>28</sup>F. Schippan, A. Trampert, L. Däweritz, and K.H. Ploog, *J. Vac. Sci. Technol.* **17**, 1716 (1999).  
<sup>29</sup>A. Trampert, F. Schippan, L. Däweritz, and K.H. Ploog, *Inst. Phys. Conf. Ser.* **164**, 305 (1999).

- <sup>30</sup>H. Okamoto, *Bull. Alloy Phase Diagrams* **10**, 549 (1989).
- <sup>31</sup>H. Okamoto, *Binary Alloy Phase Diagrams* (American Society of Metals, Metals Park, OH, 1990), Vol. 1, p. 293.
- <sup>32</sup>K. Adachi and S. Ogawa, in *Magnetic Properties of Non-Metallic Inorganic Compounds Based on Transition Elements*, edited by H. P. J. Wijn, Landolt-Börnstein, New Series, Group III (Springer-Verlag, Berlin, 1988), Vol. 27, pt. a, p. 148.
- <sup>33</sup>C.P. Bean and D.S. Rodbell, *Phys. Rev.* **126**, 104 (1962).
- <sup>34</sup>I.M. Vitebskii, V.I. Kamenev, and D.A. Yablonskii, *Fiz. Tverd Tela (Leningard)* **23**, 215 (1981) [*Sov. Phys. Solid State* **23**, 121 (1981)].
- <sup>35</sup>S. Adachi, *J. Appl. Phys.* **58**, R1 (1985).
- <sup>36</sup>A.J.P. Meyer and P. Taglang, *J. Phys. Radium* **14**, 82 (1953).
- <sup>37</sup>N.P. Grazhdankina and A.M. Burhanov, *Zh. Eksp. Teor. Fiz.* **50**, 1519 (1966).
- <sup>38</sup>B. Jenichen, R. Köhler, and W. Möhling, *J. Phys. E* **21**, 1062 (1988).
- <sup>39</sup>S.N.G. Chu, A.T. Macrander, K.E. Stege, and W.D. Johnston, *J. Appl. Phys.* **57**, 249 (1985).
- <sup>40</sup>G.G. Stoney, *Proc. R. Soc. London, Ser. A* **32**, 172 (1909).